A Comparison of Airload Data Between Model-Scale Rotor And Full-Scale Flight Test

Chee Tung and William G. Bousman
Research Scientist
Army Aeroflightdynamics Directorate, AVRDEC, ATCOM
Ames Research Center
Moffett Field, California
and
Scott Low
Research Scientist
Sterling Software
NASA Ames Research Center
Moffett Field, California

Abstract

Test data obtained from the NASA/Army UH-60A Airloads Program have been compared with measurements from the wind tunnel test of a model of the UH-60A helicopter main rotor. The airloads from hover, level and descent flights were examined and compared. The difficulty of obtaining identical matching conditions is demonstrated, in part because of the inaccuracies of the measurement of rotor lift from flight test. However, it is possible to compare close or similar condition and those comparisons provide insight into the aerodynamic environment of the rotor. For the level flight case, both model-scale and full-scale rotor blades at high advance ratio exhibit negative lift during the second quadrant and the interaction by a pair of vortices of opposite strength. In hover, the normal force coefficients for the flight test are not as steady as the model rotor test even though the ambient wind condition is less than one knot. The influences of the fuselage, tailboom, and tail rotor on the normal force are observed for the full-scale flight case. For the descent flight, the airloads due to blade-vortex interaction are similar in general but differ in details such as locations and amplitude.

Presented at the American Helicopter Society Aeromechanics Technology and Product Design, October 11-13, 1995

List of Symbols

c	= chord
C_n	= rotor sectional normal force coefficient
C_Q	= rotor torque coefficient
C_T	= rotor thrust coefficient
C_t	= rotor sectional thrust coefficient
C_W	= weight coefficient
FM	= figure of merit $= C_T^{3/2}/\sqrt{2}C_Q$
GW	= gross weight
L_F	= fuselage lift
L_S	= stabilator lift
$L_{T/R}$	= lift from canted tail rotor
M	= local Mach number
r	= rotor radial section
R	= rotor radius
x	= chordwise location
α_{TPP}	= tip path plan angle of attack
α_s	= shaft angle of attack
β_{1c}	= longitudinal flap angle
γ	= descent angle
μ	= advance ratio
ψ	= azimuth angle
σ	= solidity

Introduction

Model rotor tests have been widely used as a research tool to study many problems encountered by the helicopter in areas dealing with aerodynamics, dynamics, and aeroacoustics, just to name a few. Relative to flight test, it is cost effective to test model rotors in the wind tunnel to evaluate the effects of changes in blade geometry, airfoil, twist distribution, and planform. The incremental trends as compared with the baseline rotor are then used for the adjustment of the rotor performance. Ref. 1 has discussed the requirement of geometric and dynamic scaled rotor blades and operation at full-scale tip Mach number for a meaningful scaling of the performance data. The effect of Reynolds number on the profile power can be obtained using a simple power law. The scaling techniques were correlated using 1/6-scale CH-47D wind tunnel data with full-scale CH-47D whirl tower and flight test results. In Refs. 2 and 3, the authors presented the performance results of a 1/5-scale model rotor with a scaled fuselage, full-scale isolated rotor with a generic fuselage, and full-scale flight-test. The full-scale isolated power coefficient over solidity agrees well with the flight-test data, but both differ from the model-scale rotor by a constant value when the rotors were operated below the stall condition. No scaling law is required for this rotor.

Recently, a large quantity of airload measurements have been obtained for a 1/5.73-scaled pressure-instrumented model of the UH-60A main rotor without a fuselage at the Duits-Nederlandse Wind Tunnel (DNW). The blades are geometrically and dynamically scaled. A total of 176 pressure transducers, 16 strain gauges, 8 temperature detectors, and 12 hot film anemometers was installed on four different blades. The test (Ref. 4) included hover, level fight, and descent conditions. Subsequently, a UH-60A Black Hawk with an extensively instrumented rotor has been flown to obtain complementary airload data (Ref. 5). One of the blades has a total of 221 pressure transducers installed in nine spanwise stations similar to that of the model-scale rotor. The second blade was installed with strain gauges and accelerometers to measure the structural loads and response of the blade. The testing included hover, level flight, and descent flight conditions. There are many flight conditions that are common to both the model-scale wind tunnel and the full-scale flight test (Ref. 6).

This paper will attempt to address three issues in terms of correlation between model and full-scale data. First, can direct comparison of wind-tunnel and flight conditions provide information on scaling of rotor performance? Second, do the different trim procedures used in model and flight tests substantially and quantitatively affect the airloads? Third, is there a one-to-one correspondence for BVI amplitudes and locations between model-scale and flight tests.

Matching of Test Conditions

Level flight data were obtained for the model-scale rotor test by selecting nondimensional values of rotor lift and propulsive force and varying advance ratio. The lift and propulsive force were measured with a rotor balance and collective and shaft angle were used to obtain the selected forces at each advance ratio. The cyclic control angles were adjusted to zero out the first harmonic of blade flapping. For the flight test program data were obtained over a range of advance ratios as well, but for a constant weight coefficient, C_W, rather than lift or thrust coefficient, C_T. Cyclic controls were used to trim the aircraft moments and the flapping angles and shaft angles were not controlled.

Hover data were obtained on the model-scale rotor over a range of thrust values, again with zero harmonic flapping, and with little influence of external factors such as winds and recirculation. Hover data for the flight test program were only obtained for a limited range of gross weight. In all cases the influence of the tail rotor was present and in most cases there was some degree of crosswind. Cyclic controls were adjusted to trim the aircraft moments to zero, but this resulted in non-zero values of first harmonic flapping.

For descending flight conditions during the model-scale test, an advance ratio and lift coefficient were selected. Then, the shaft angle was used to vary the effective inflow through the rotor to simulate various descent conditions. For the flight test program the aircraft was flown for a matrix of airspeeds and descent angles but no attempt was made

to keep the weight coefficient constant. The aircraft ILS director was driven by a pre-programed descent path and a laser tracker was used to measure the aircraft displacements.

It is unlikely that any two test conditions can be obtained from the model-scale and flight test data that are an exact match. In part, this is a consequence of the order of the tests as the model-scale test were performed first and it is not possible in flight to match wind-tunnel trim conditions. However, the greatest difficulty in obtaining matching data is probably the uncertainty in the rotor lift. In the model-scale tests rotor lift was measured with a rotor balance and this was compared to an integration of the pressures on the blade and agreement was within 1-2% (Ref. 7). For the flight test program, conditions were set on the basis of weight rather than rotor lift and the difference is shown in the vertical force balance equation

$$T\cos\alpha_s - GW = -L_F - L_s - L_{T/R} \qquad (1)$$

where the fuselage lift, the stabilator lift, and the lift from the canted tail rotor will cause a difference between the rotor lift and the aircraft gross weight. In hover there is download on both the fuselage and the horizontal stabilator, while the tail rotor provides a lift force because of its canted design. The download, negative L_F and L_s, is not easily estimated but is expected to be 4% or greater (Ref. 8). The tail rotor lift is related directly to the main rotor torque and is about 2.5% in hover. The rotor thrust in hover, therefore, will be greater than the gross weight. As advance ratio increases the rotor downwash will move aft on the fuselage and the rotor wake-induced download will decrease. The tail rotor lift will also decrease as main rotor torque is reduced with forward speed and the thrust is expected to remain greater than the gross weight. At moderate speeds, as the dynamic pressure increases and the fuselage and stabilator lift forces become effective then wind tunnel data (Ref. 9) can be used to estimate these forces and the primary source of inaccuracy at this point becomes the calculation of angle of attack correction terms related to the rotor wake (Ref. 3). At these speeds the main rotor thrust is expected to be slightly less than the gross weight. Between $\mu = 0.15$ and $\mu = 0.25$, depending upon the influence of the rotor wake, the effective fuselage and stabilator angles of attack become negative. The download associated with fuselage and stabilator will be greater than the lift produced by the tail rotor. Thus, the rotor thrust will again be greater than the aircraft weight. Near the maximum speed of the aircraft, $\mu = 0.35$, the calculated download is approximately 9% and the tail rotor lift is 3%, hence the thrust is calculated to be 6% greater than the aircraft weight. The integration of the flight test blade pressures indicates an excess of rotor lift over aircraft weight of from 5 to 15%, depending upon operating condition, and a substantial fraction of this excess cannot be explained by the effects of the fuselage, stabilator, and tail rotor forces.

Previously, Ref. 5, level flight conditions at $\mu = 0.3$ were compared for the model-scale and flight test data (13.10/8424 – in this paper test conditions comparisons are shown by listing the model-scale run.point number first, followed by a slash, and then the flight test counter number). However, for the level flight comparison point examined here a slightly higher thrust condition will be used (13.20/8424) as shown in Table 1. In addition to this comparison point, the performance in level flight will be compared over a range of airspeeds.

During the ground acoustics portion of the UH–60A flight test program (Ref. 5) a considerable amount of hover data was obtained where the aircraft ground velocity was accurately known, based on laser and radar tracking, and the air mass velocity at the aircraft elevation was known from tethered balloon measurements. The comparison selected (34.03/9605) represents a flight test case with less than one knot motion of the vehicle with respect to the air mass. A comparison of the two test conditions is shown in Table 1.

A number of cases in descending flight were compared by Rutledge *et al.* in Ref. 6. These cases were selected primarily by matching advance ratio and the calculated tip-path-plane angle. These cases are used again for the present paper with the addition of a $\mu = 0.20$ condition as shown in Table 1.

Level Flight

Level flight performance data are compared in

Fig. 1 for nominal model-scale conditions of $C_T/\sigma = 0.09$ and $\overline{X} = 0.10$, and flight conditions of $C_W/\sigma = 0.09$ (Flight 84). The C_P/σ for the wind tunnel test are slightly higher than the flight test data at the lower advance ratios, and then become lower at the highest advance ratio. The two sets of data are similar although, as discussed previously, it is not possible to obtain a direct match between the two sets of test conditions.

The selected level flight condition from the model-scale test is not the $\mu = 0.3$ point from Fig. 1 (13.10), but rather a condition from a $C_T/\sigma = 0.10$ airspeed sweep (13.20), where the the C_P/σ value is closer to the flight condition. The normal forces at eight radial stations for these two cases (13.20/8424) are shown in Fig. 2. The model-scale data are the average of 64 revolutions of data while the flight test data are a single revolution. Generally, the measured normal force data are similar but there are differences in a number of areas. Directly over the tail, $\psi = 0°$, the wind tunnel data show less lift and this is particularly noticeable inboard on the blade. It seems likely that this lift deficiency is related to the separated wake behind the larger instrumentation beanie on the model rotor. An increased variance in the measured pressures was noted in Ref. 6 in this area. Both sets of data show extensive regions of negative lift outboard of $0.865R$, but the lift on the model rotor is more negative than in the flight test and also extends over a greater azimuthal range.

Both sets of data show an increase in lift at the end of the first quadrant on the outer portion of the blade ($r/R \geq 0.865$) that is quite short in duration. It appears that this loading is vortical in nature and is, in fact, partly a result of a secondary trailing vortex combined with the "tip vortex." Fig. 3 shows the radial distribution of normal force at $\psi = 90°$, just before the lift becomes negative and at $\psi = 135°$, where the lift is most negative. The lift distribution at 90° is positive with the peak lift inboard from the blade tip and it is expected that the trailed vorticity will rapidly form a tip vortex which, when viewed from behind the blade, will have a counterclockwise (CCW) rotation. At 135° there is a substantial area of negative lift on the outer portion of the blade and the model-scale data shows a greater extent of this negative lift region. In this region it is not unreasonable to expect the trailed vorticity to roll up into two tip vortices, the outer one with CW rotation and the inner one with CCW rotation. Such a vortex pair has, in fact, been visualized using a laser light sheet on a BO-105 model-scale rotor(Ref. 10).

Assuming that a pair of vortices of opposite sign and comparable strength are trailed from the rotor in the second quadrant then, depending upon how these vortices are convected by the mean inflow they will intersect the following blade in the first quadrant. Fig. 4 shows the upper surface pressure at $0.01c$ at the 92% radial station for this level flight condition. Both sets of data show a disturbance in the pressure near 90°. In both cases it appears that this disturbance is caused by a localized upwash at the leading edge of the blade. A close vortex pair, as discussed above, would cause a downwash both in front and behind the vortex pair, while in between would be an upwash region and this upwash region is believed to be the source of the increased loading shown in Fig. 4. With the increased resolution of the model-scale measurements, it is possible that the loading of the individual vortices is discernible in the figure.

The presence of a tip vortex of opposite sign to the normal tip vortex, created in the region of negative lift on the advancing side, was proposed in Ref. 11 to explain the loading observed on the CH–34 rotor. Modeling of this kind of lift distribution, the so-called "dual-peak" model, has been added to the CAMRAD/JA code (Ref. 12) and clearly both the model-scale and full-scale data will provide good tests of these modeling features. How important this type of loading is for rotor vibration and acoustics in high speed flight conditions remains to be determined.

The comparisons shown here for the level flight comparison case (13.20/8424) show good qualitative agreement, even down to the level of the vortex loading induced by the region of negative lift near the blade tip on the advancing side. However, these two cases are not exactly matched in terms of global trim parameters and at the quantitative level there are clearly numerous small differences in the inflow on the rotor and these difference vary over the blade span and azimuth.

The level flight comparisons shown here, both in

terms of general performance, as seen in Fig. 1, or the airloads, as in Fig. 2, do not have the accuracy required to derive appropriate scaling laws. The effects of Reynolds number, for instance, appear to be of the same order as discrepancies in the parameters that define the matching conditions between model-scale and flight test. The approach used in Ref. 3, where extensive performance data are obtained and used as a data base for interpolation, remains the best method for quantifying the effects of scaling parameters.

Hover Condition

The comparison case shown here (34.03/9605) is for $C_T/\sigma \approx 0.066$ and the flight case, as discussed previously, is one of the test conditions obtained in the test program where the aircraft motion relative to the air mass is less than one knot. The hover tip Mach number for the model-scale data is slightly higher than the flight case (Table 1), but this effect is slight for hover Mach numbers less than 0.7.

The sectional normal force, M^2C_N, is shown in Fig. 5 for eight radial stations from $0.40R$ to $0.99R$. The model-scale data shown are an average of 64 revolutions, while the flight test data are averaged over 16 revolutions. A single revolution of flight test data is included as well to indicate the large load variation that is observed in the full-scale data.

Inboard on the blade, similar lift levels are seen for the model-scale and flight-test data. From $0.865R$ to $0.92R$ the model scale data show more lift than on the full-scale rotor, while at $0.965R$ and $0.99R$ the converse is true. On the inboard portion of the blade the flight test data show a slight increment in lift at 0° and 180° which is likely the effect of the fuselage. Substantial unsteadiness is observed in the flight-test data both in the third and fourth quadrants and as far inboard as $0.775R$. These rapid, large lift variations can possibly be explained by interaction of the blade with portions of the main rotor vortices or, possibly, the tail rotor tip vortices.

The Figure of Merit (FM) for Counter 9605 is compared with a range of model-scale data in Fig. 6 using three different assumptions. The highest FM point, $C_T/C_W = 1.14$, is calculated based on the integrated blade pressures, and the resulting value is well above the faired model-scale curve. If the thrust is estimated assuming a download of 4% and a tail rotor lift of 2.5% then $C_T/C_W = 1.015$ and the Figure of Merit is similar to the model-scale data. The third FM point is based on assuming that the rotor thrust and aircraft weight are the same and this gives a value below the model-scale data. It seems clear from this comparison of isolated model-scale rotor data with flight test data that the former approach is the best means of obtaining detailed information on hover performance. However, the flight data clearly show the influence of installation and interference effects and how important it is to include these in the final performance calculations.

Descending Flight

Four descent cases were selected for comparison. The test conditions are listed in Table 1 and are compared on the basis of tip-path-plane angle of attack, α_{TPP}, in Fig. 7. For the model-scale data α_{TPP} was computed based on the shaft angle of attack and the measured blade flapping, that is, $\alpha_{TPP} = \alpha_s - \beta_{1c}$. The first harmonic cosine flapping was, in general, less than 0.1°. α_{TPP} was computed for the flight test data from the measured pitch attitude, the first harmonic flapping, and the descent angle determined from measured forward speed and rate of descent, that is, $\alpha_{TPP} = \alpha_s - \beta_{1c} - \gamma$. The first harmonic cosine flapping for the flight test data ranged from 1.5° to 2.2°. This approach differs from the one used in Ref. 6 and the match in α_{TPP} is not as good as shown there.

The four descent cases, $\mu = 0.15$ to 0.3 are compared in Fig. 8. As before, the model-scale data are an average of 64 revolutions of data while the flight test data are shown for a single revolution. As in the level flight comparison the normal forces as a function of an azimuth and radial station are similar overall but show a number of detailed differences. The flight test normal force at $0.40R$ and $\mu = 0.20$ is not considered trustworthy, but the normal force at this radial station for the other advance ratios shows a positive shift in the airloads and this may be an effect of the fuselage. Further outboard on the blade the steady component of lift shows better agreement between the model-scale and flight test data. The trim differences between the two sets of data

as evidenced by the lower frequency airloads appear quite small except at the lowest speeds where a phase shift in the loading is seen on the front of the rotor disk. However, when the blade vortex interaction locations are examined it can be seen that there are significant differences in phase and amplitude of the various vortex interactions. These details are shown more clearly in Fig. 9 where the first 16 harmonics of the data have been removed from the measured airloads at $0.92R$. Although the signal strength and number of interactions are comparable between the two data sets there are numerous difference in phase and amplitude. In some cases, such as on the advancing side for $\mu = 0.20$, prominent vortex interactions are seen in the wind tunnel data, while the flight test data show only very low amplitude loads. Similarly, at $\mu = 0.30$, the flight test data show a series of quite strong interactions on the retreating side that are not observed in the model-scale data. These high-frequency airloads are sensitive to the exact location of the blade vortices and it is clear that the approximate match between the model-scale and flight test conditions does not provide a perfect one-to-one correspondence.

As reported in Ref. 13, one may use the valley/peak from the leading edge pressure measurements along the rotor span over the advancing and retreating sides to identify the measured BVI locations. Therefore, the BVI locations from the leading edge pressure measurements were obtained and are plotted in Fig. 10. The number of BVI reduces as advance ratio increases for both the flight and model rotor tests. The phase shift in the BVI locations is clearly shown in this figure. The difference in trimming the rotor for the model-scale test and the flight test does not affect the number of BVI in general but does affect the magnitude of the normal forces.

Concluding Remarks and Recommendations

Model-scale wind tunnel test data and full-scale flight-test data have been compared for the UH-60A to include both standard performance measurements and blade airloads as determined by surface pressures. The comparisons have been made for level flight, hover, and descent flight conditions. Obtaining an exact match or one-to-one comparison between model-scale and flight-test conditions is difficult and, therefore, it is not possible to derive scaling effects or laws between model scale and full scale. The greatest difficulty encountered in the comparisons is the determination of rotor thrust on the test aircraft and differences between rotor thrust determined by pressure integration and by a force balance equation are unresolved. The comparisons are also made more difficult by differences in the methods of trim used for the model and flight tests. The effects of these trim differences were not quantified in the comparisons.

Comparison of BVI conditions in descending flight over a range of advance ratios show quantitative differences in the amplitude and phase of specific BVI interactions and it is expected that these quantitative differences will also be seen in the acoustic data, although that remains to be demonstrated. Both sets of data will provide valuable tests for the developer of analytical methods and are highly complementary in the sense that the steadiness of the wind tunnel data.

Although the comparisons shown in the paper fail to meet the quantitative objectives set forth, they do show excellent qualitative agreement for the majority of cases, and where differences occur, these differences provide a great deal of information relative to model-scale to full-scale correlation. For the level flight at higher advance ratio, the blades exhibit negative loading for both flight and model-scale test in the second quadrant. The interaction of dual vortices of opposite strength with the blade occurs near $\psi = 90°$ azimuth angle as shown by the leading-edge surface pressure near the blade tip. For the hover case, the airloads measured from the flight test are strongly influenced by the fuselage, tailboom, and tail rotor in contrast to model-scale rotor. For the descent flight, the airloads due to BVI are similar between the flight and model-scale tests. However, the amplitudes and locations of each interaction are quite different.

The comparisons shown here also suggest that the classical approach of model testing, using a rotor without pressure instrumentation but with a scaled fuselage, stabilator, and tail, remains the best way to obtain performance data in hover and forward

flight. The role of the pressure-instrumented rotor lies in the understanding of conditions where analytical methods are less accurate and particularly for conditions where the influence of vorticity in the rotor wake is pronounced. Future model-scale tests should, however, include more derivative-type testing to better quantify the effects of rotor trim. Future flight tests, on the other hand, should measure the main rotor thrust directly or the thrust be derived accurately from other means. Finally, some of above mentioned questions may be better answered by the coming full-scale rotor test in the 40X80 wind tunnel. The full-scale rotor can be trimmed either to zero flapping as the model-scale rotor or to a given flapping angle as the flight test. The rotor thrust will be measured by the balance system or from the integration of the surface pressure.

Acknowledgments

The authors would like to thank Peter Lorber of UTRC for his valuable suggestions throughout the course of this work. We would also like to thank M. Silva of AFDD for his assistance.

References

[1] Keys, C. N.; McVeigh, M. A.; Dadone, L. U.; and McHugh, F. J.,"Estimation of Full-Scale Rotor Performance from Model Rotor Test Data", Journal of American Helicopter Society, Vol. 30, No. 4, Oct. 1985.

[2] Balch, D. T., "Correlation of Full Scale Wind Tunnel Test Data with model Rotor Test Data and Theory for a Morden Helicopter Main Rotor", Journal of American Helicopter Society, Vol. 24, No. 2, July 1979.

[3] Jepson, D.; Moffitt, R.; Hilzinger, K.; and Bissell, J.,"Analysis and Correlation of Test Data from an Advanced Technology Rotor System", NASA CR-3714, August 1983.

[4] Lorber, P. F., "Aerodynamic Results of a Pressure-Instrumented Model Rotor Test at DNW, presented at 46th Annual Forum of the American Helicopter Society, Washington D. C., May 1990.

[5] Kufeld, R. M.; Balough, D. L.; Cross, J. L.; Studebaker, K. F.; Jennison, C. D.; and Bousman, W. G., "Flight Testing of the UH-60A Airloads Aircraft", presented at 50th Annual Forum of the American Helicopter Society, Washington D. C., May 1994.

[6] Rutledge, C. K.; Mueller, A. W.; and Wilson. M., "A Study of the Variability Difference Between Model Scale Wind Tunnel and Full Scale Flight Test Airloads Data", presented at the American Helicopter Society Vertical Lift Aircraft Design Conference, San Francisco, CA, January 1995.

[7] Lorber, P. F., Stauter, R. C., Pollack, M. J., and Landgrebe, A. J., "A Comprehesive Hover Test of The Airloads and Airflow of an Extensively Instrumented Model Helicopter Rotor," (Volume I-IV), USAAVSCOM TR89-D-28A, B, C, D,1990.

[8] Flemming, Robert J. and Erickson, Reuben E., "An Evaluation of Vertical Drag and Ground Effect Using the RSRA Rotor Balance System", Journal of the American Helicopter Society, Vol. 28, No. 4, October 1983, pp. 59–67.

[9] Barnard, R., "YUH-60A/T700 IR Suppressor Full Scale Prototype Test Report", SER 70094, June 1976.

[10] Kube, R., Spletterstoesser, W. R., Wagner, W., Seelhorst, U., Yu, Y. H., Boutier, A., Michali, F., and Mercker, E.,"Initial Results from the Higher Harmonic Control Aeroacoustic Rotor Test (HART) in the German-Dutch Wind Tunnel", presented at the 75th AGARD Fluid Dynamics Panel Meeting on Aerodynamics and Aeroacoustics of Rotorcraft, Berlin, German, Oct. 1994.

[11] Hooper, W. E.; "The Vibratory Airloading of Helicopter Rotors", *Vertica* Vol. 8, No. 2, 1984.

[12] Johnson, Wayne R., "Wake Model for Helicopter Rotrs in High Speed Flight", NASA CR 177507, November 1988.

[13] Caradonna, F. X, Laub, G. H., and Tung C., "An Experimental Investigation of the Parallel Blade-Vortex Interaction", presented at the 10th European Rotorcraft Forum, The Hague, The Netherlands, August, 1984.

Table 1 Test conditions of matching flight-test and model-scale data.

Data Point	Adv. ratio	Mtip	CT/sigma*	CQ/sigma	RPM	Vo(m/s)	TTP Angle(deg)
8424(FT)	0.304	0.641	0.0888	0.00632	256.05	67.42	-4.96
13.20(M)	0.301	0.629	0.0984	0.00604	1442.00	65.00	-3.54
9605(FT)	0.000	0.651	0.0668	0.00511	258.53	0.00	2.68
34.03(M)	0.000	0.700	0.0650	0.00499	1561.67	0.00	0.00
9108(FT)	0.160	0.650	0.0659	0.00132	256.70	33.20	5.06
11.24(M)	0.150	0.644	0.0699	0.00144	1442.00	32.70	7.45
10214(FT)	0.202	0.634	0.0713	0.00230	246.80	42.00	2.21
11.37(M)	0.201	0.638	0.0702	0.00160	1454.00	43.06	3.91
9110(FT)	0.250	0.650	0.0646	0.00105	256.20	53.30	5.27
14.32(M)	0.250	0.644	0.0680	0.00132	1455.00	54.80	4.35
9122(FT)	0.300	0.650	0.0620	0.00234	256.40	65.00	0.52
13.12(M)	0.300	0.644	0.0696	0.00250	1456.00	65.40	0.11

* The flight test cases use CW/sigma.

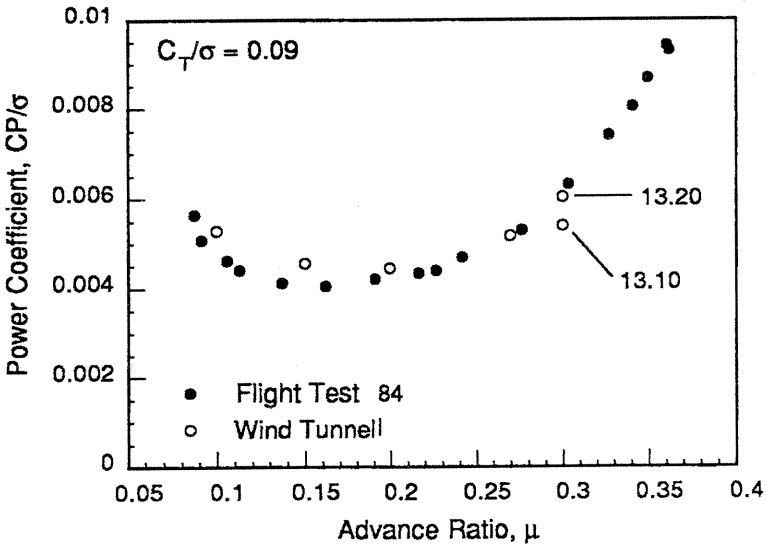

Fig. 1 Comparison of flight-test and model-scale level flight power coefficients.

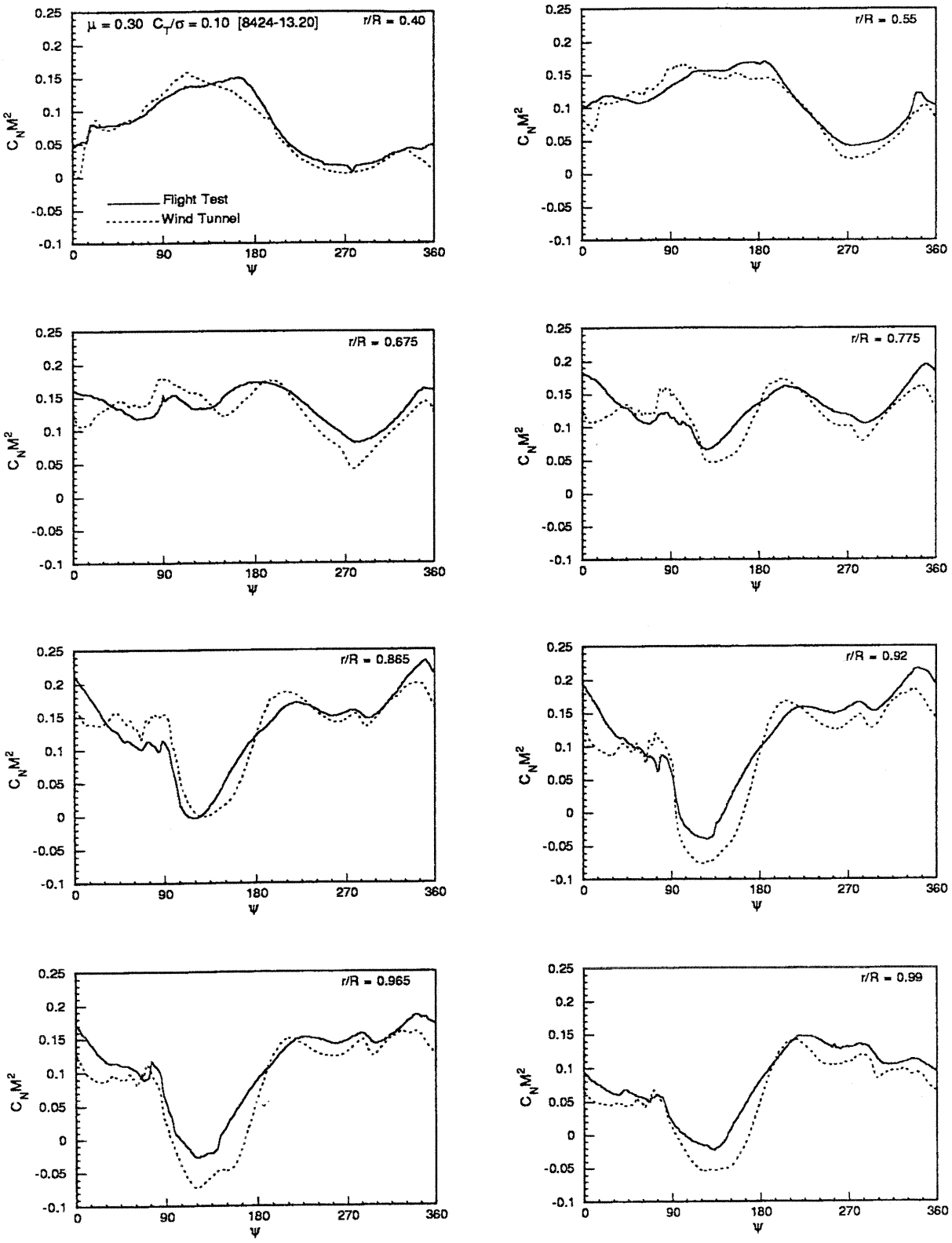

Fig. 2 Comparison of normal force for $\mu = 0.3$ and $C_T = 0.1$.

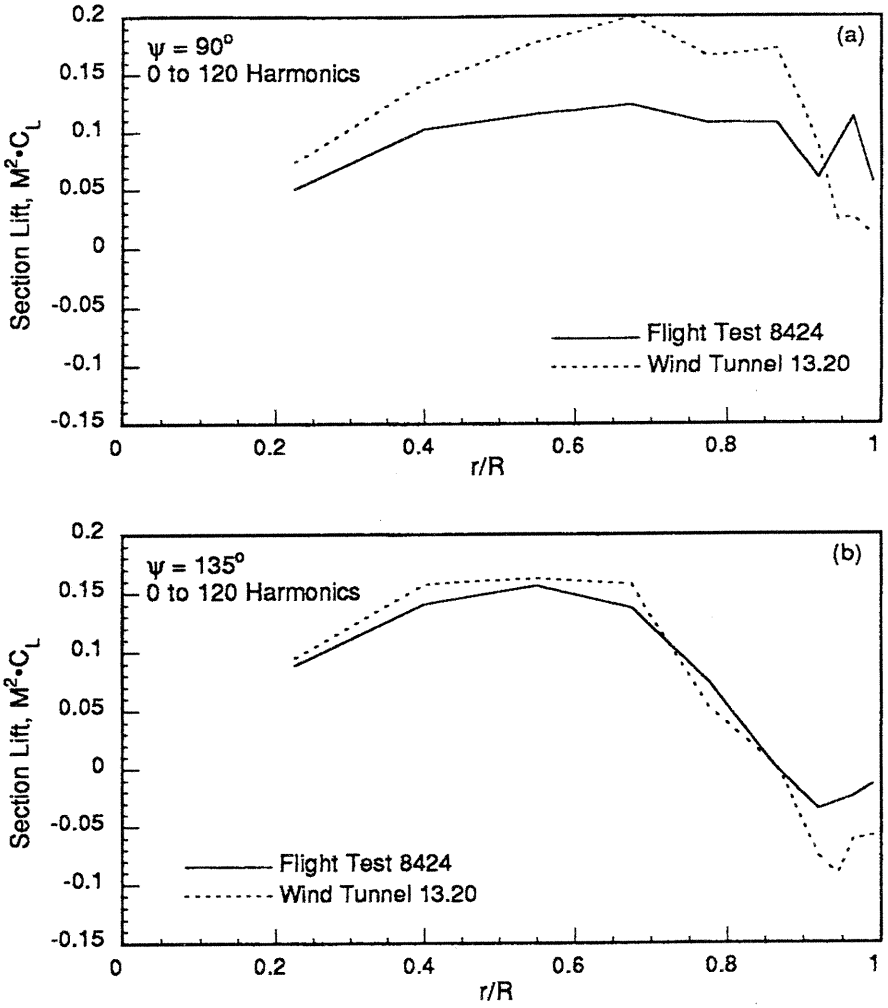

Fig. 3 Comparison of radial distribution of normal force at $\psi = 90°$ and $\psi = 135°$ for $\mu = 0.3$.

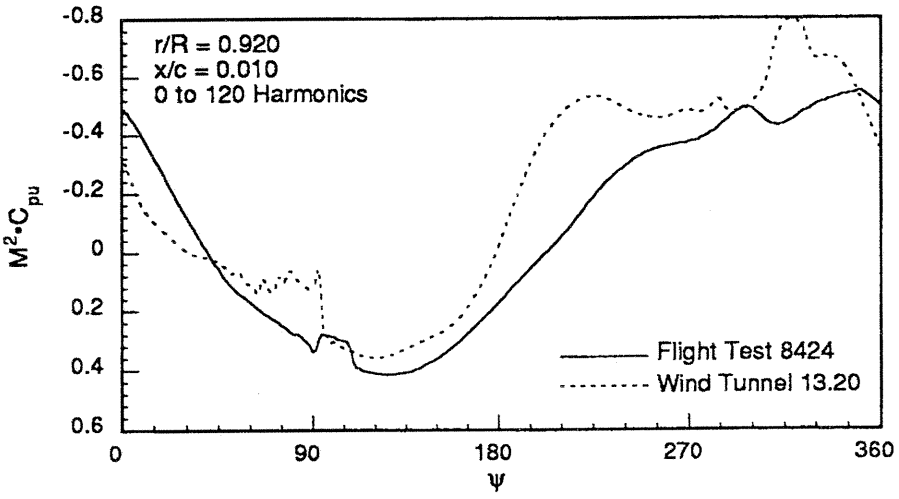

Fig. 4 Comparison of upper surface pressure at $x/c = 0.01$ and $r/R = 0.92$.

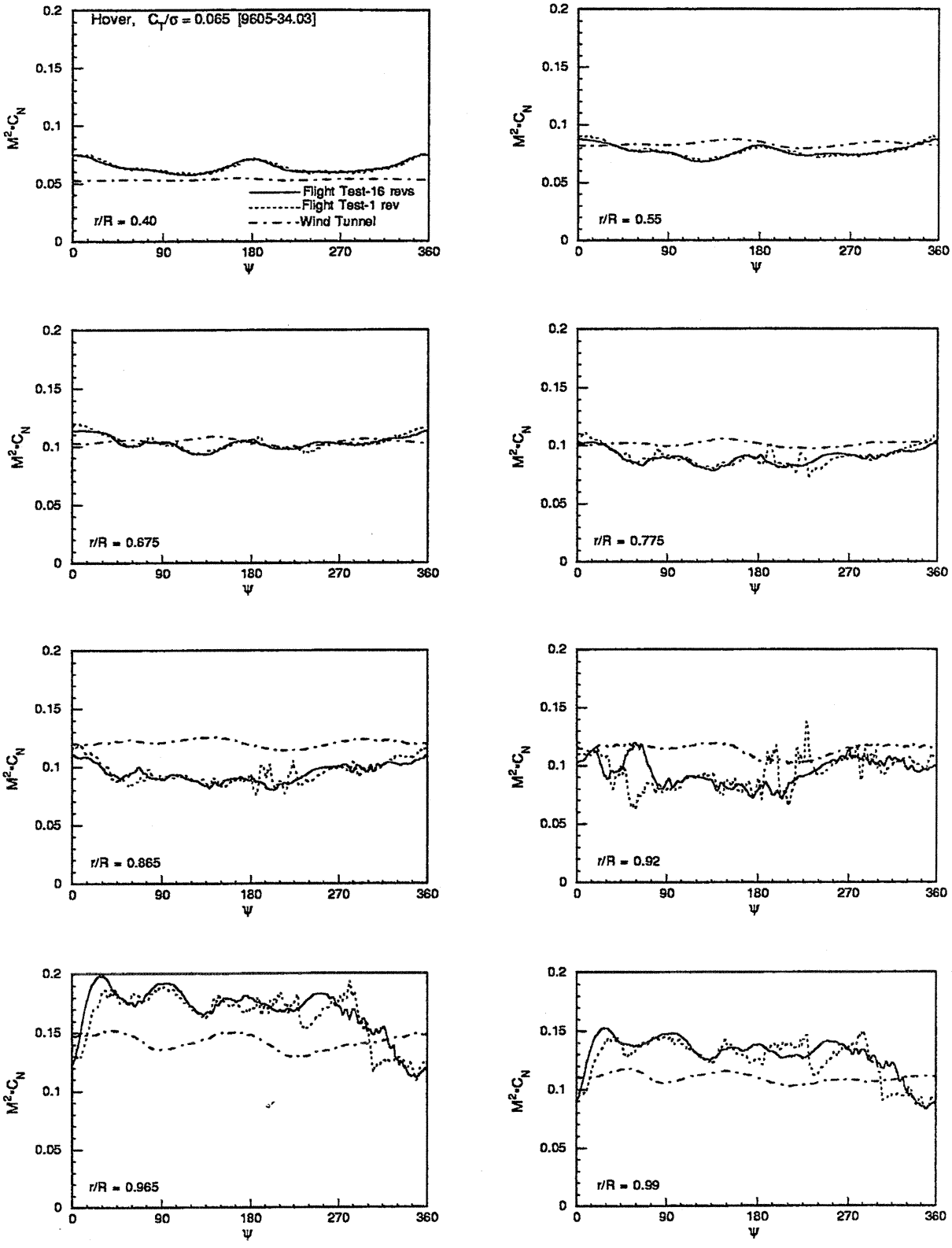

Fig. 5 Comparison of hover normal force for $C_T = 0.065$.

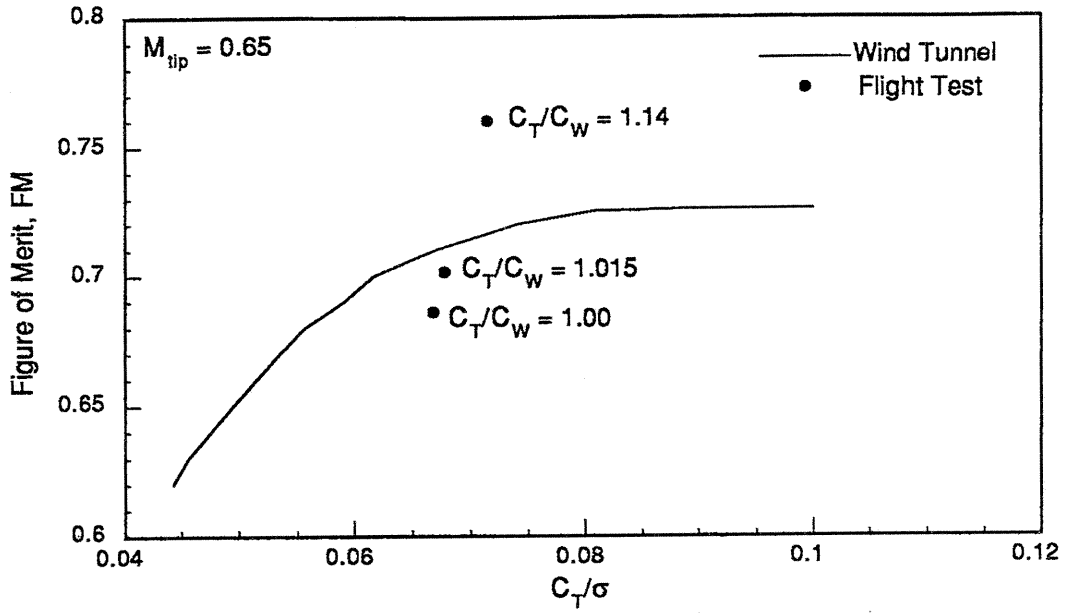

Fig. 6 Comparison of FM for Flight Counter 9605 with model-scale data.

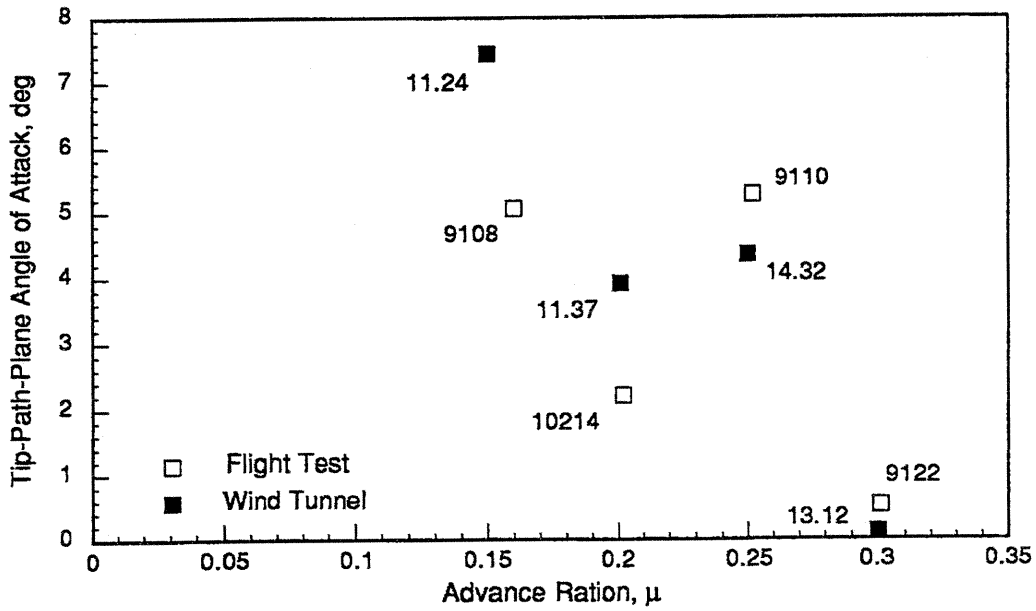

Fig. 7 Comparison of tip path plane angle of attack at four different advance ratios.

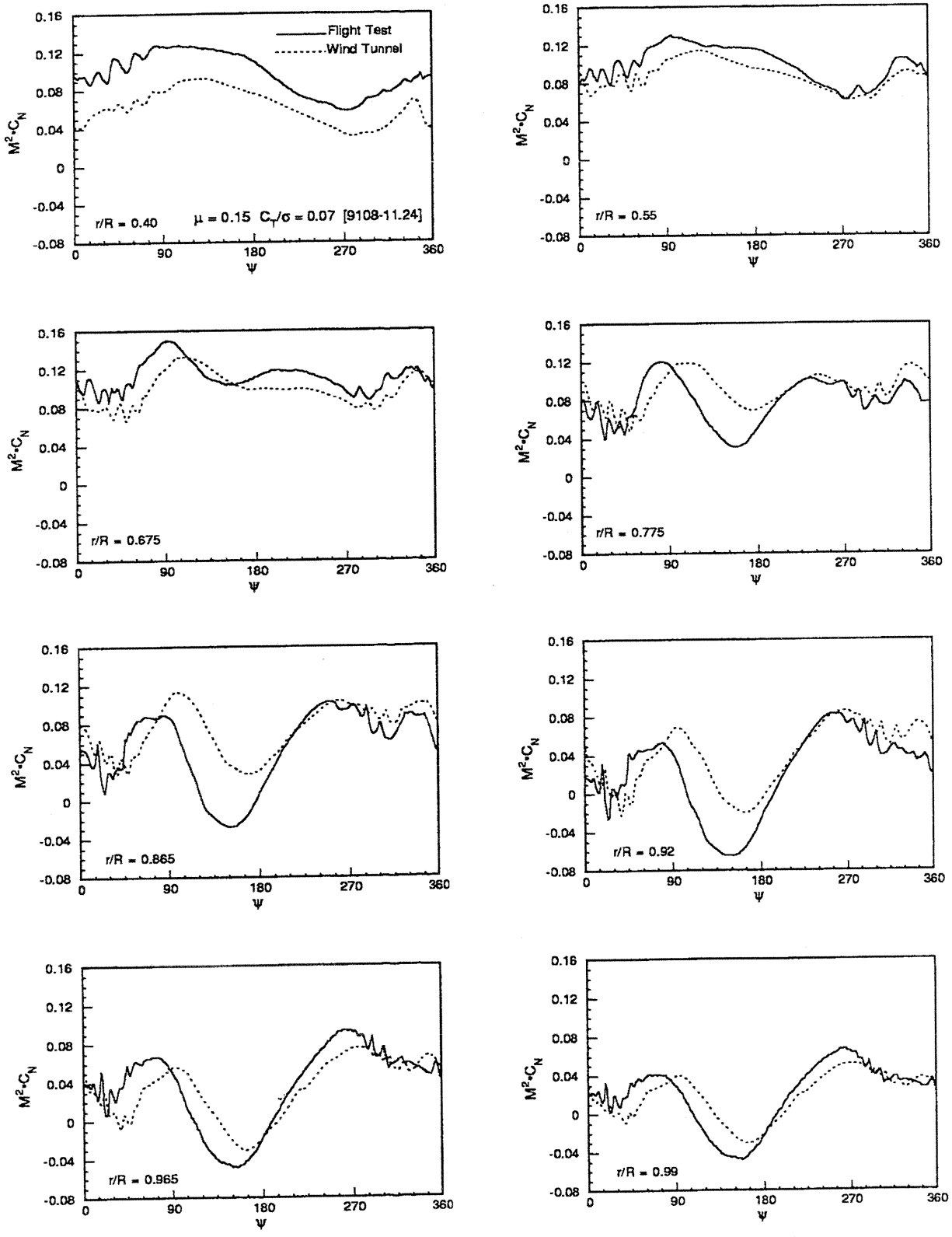

Fig. 8a Comparison of normal force at $\mu = 0.15$.

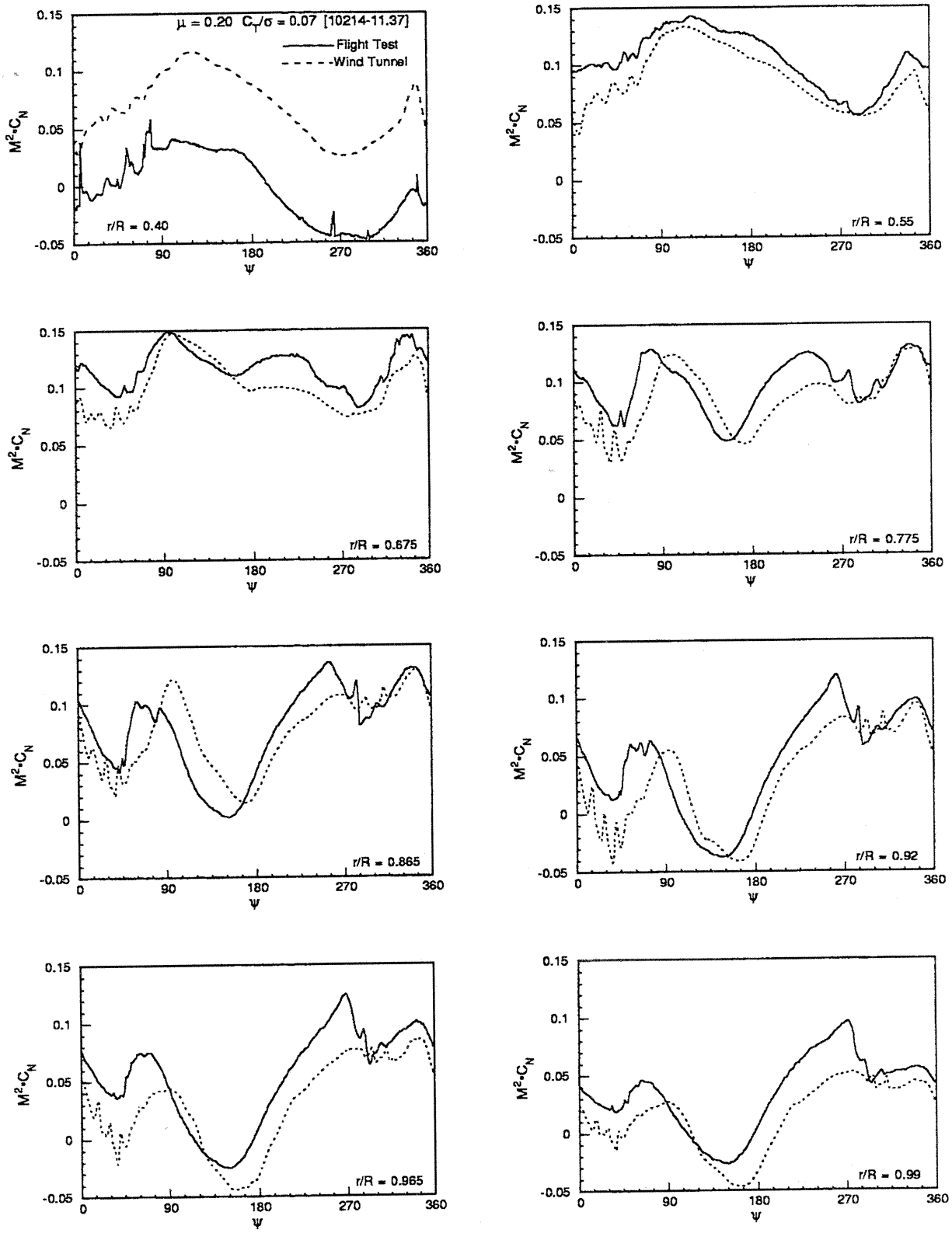

Fig. 8b Comparison of normal force at $\mu = 0.20$.

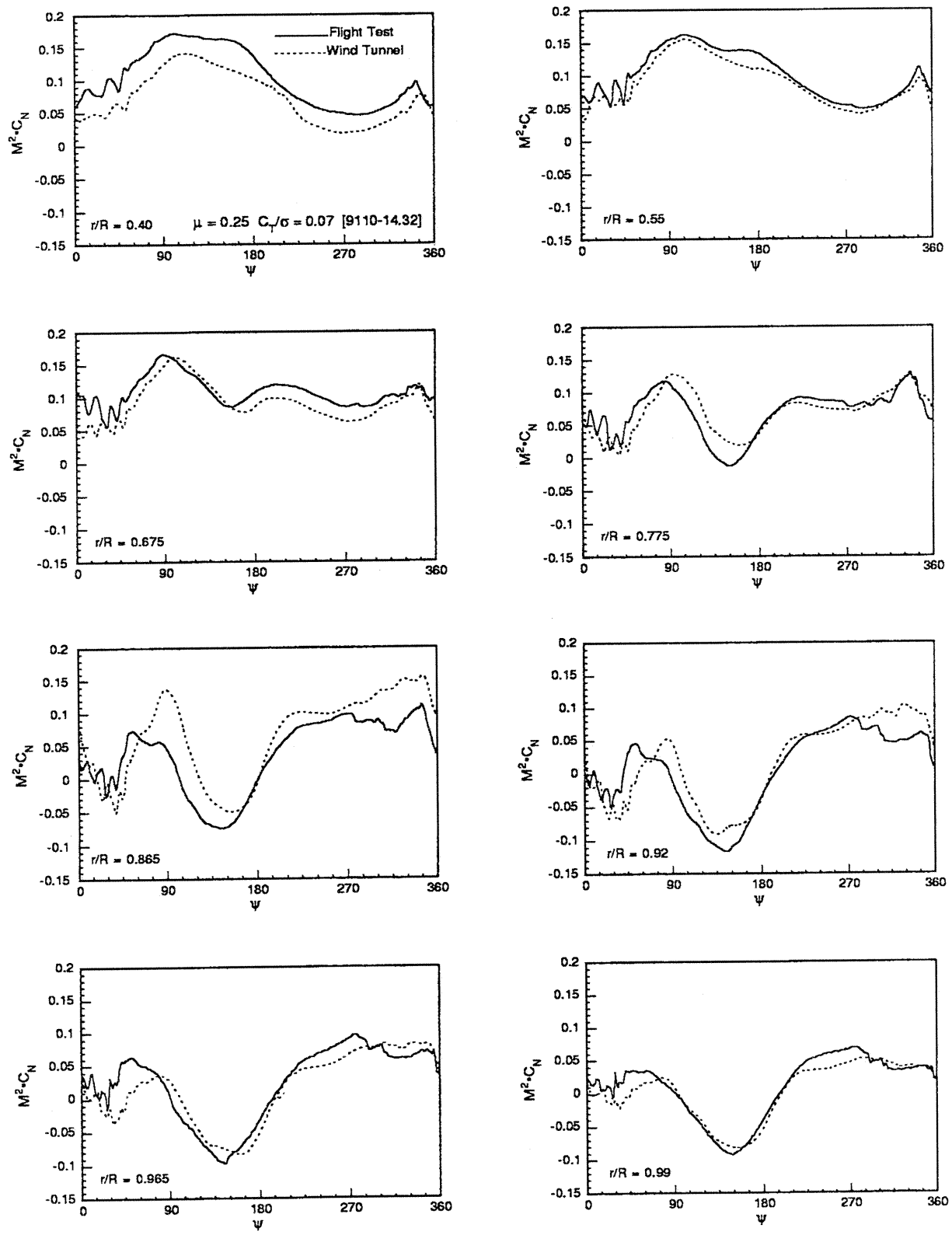

Fig. 8c Comparison of normal force at $\mu = 0.25$.

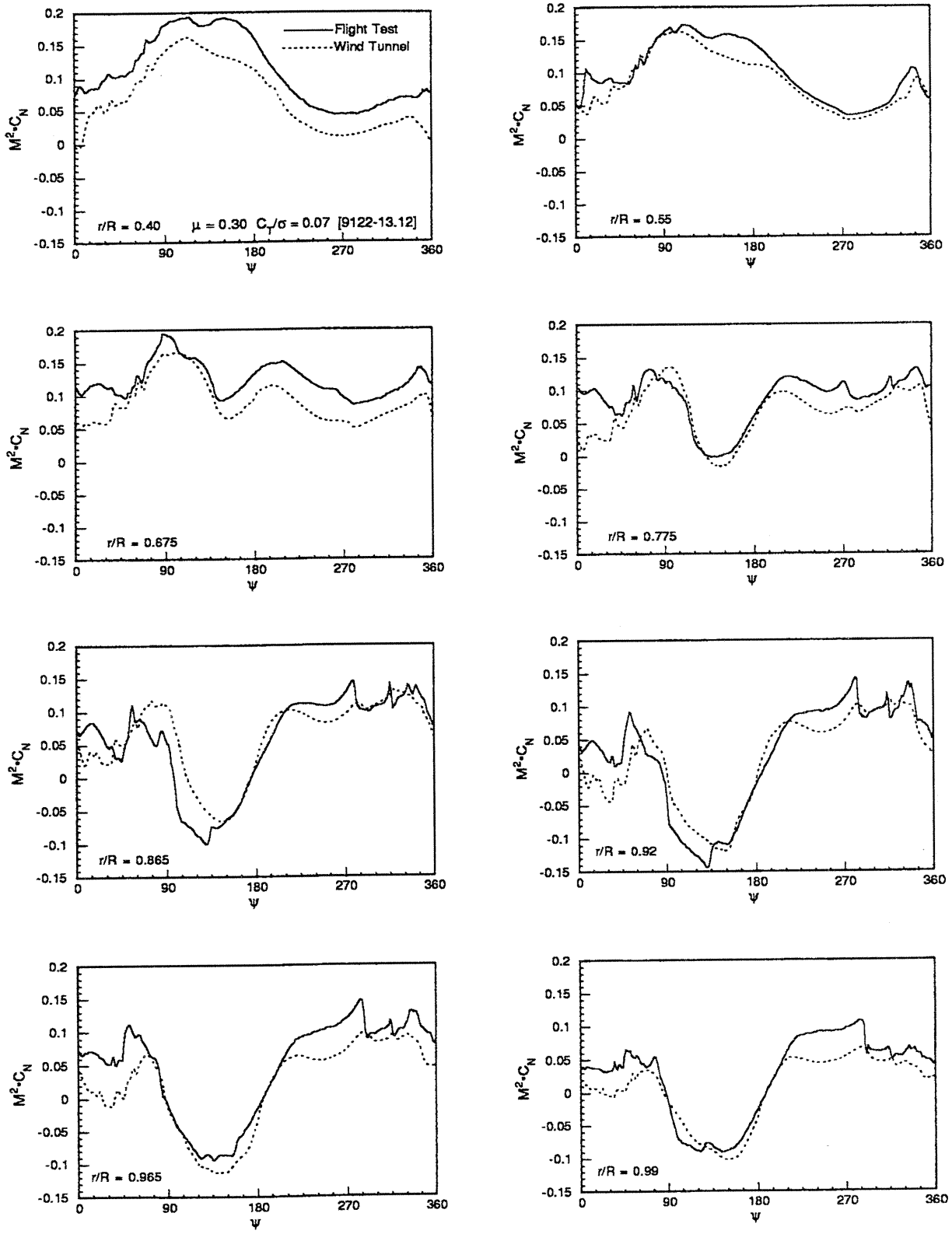

Fig. 8d Comparison of normal force at $\mu = 0.30$.

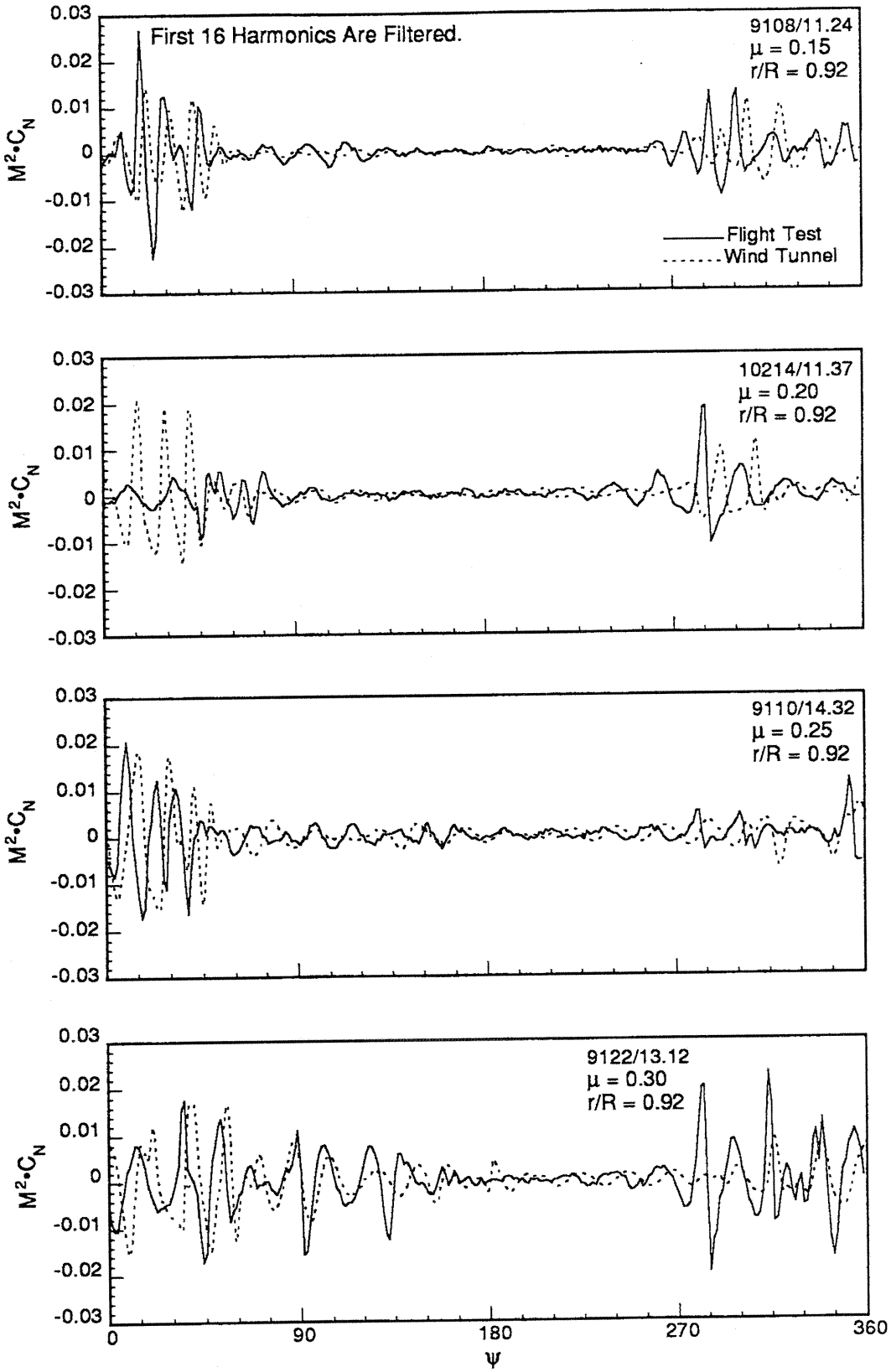

Fig. 9 Comparison of normal force at $r/R = 0.92$ for four different advanc ratios, with 0-16 harmonics removed.

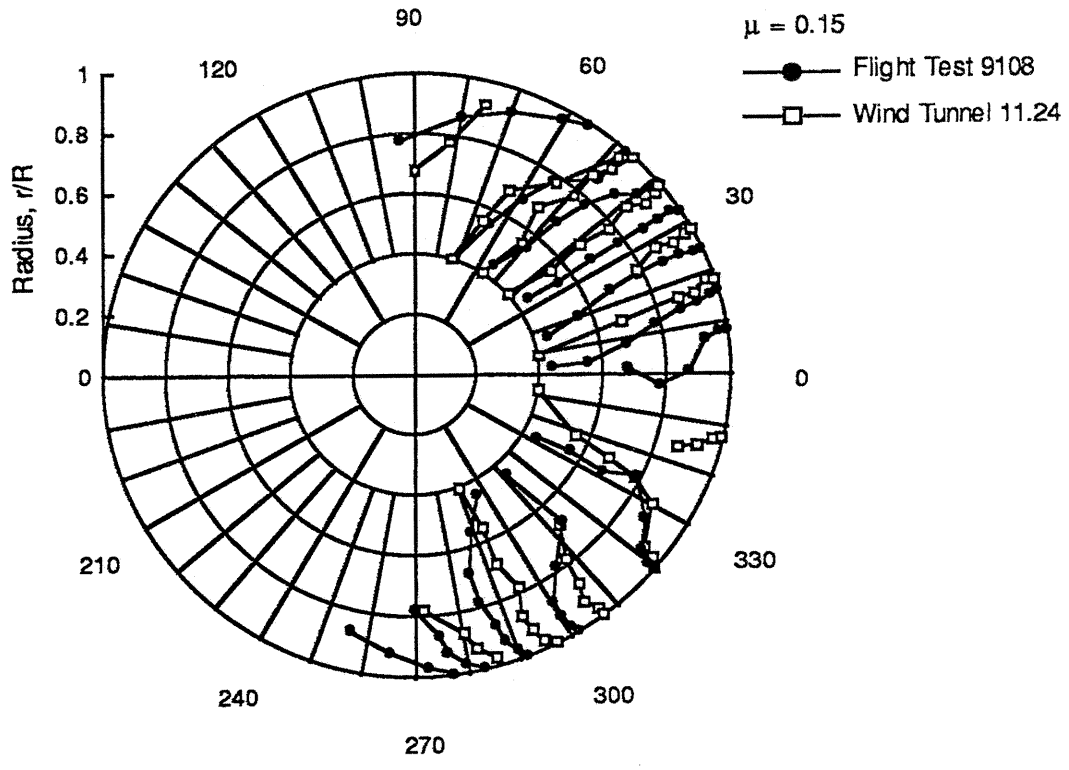

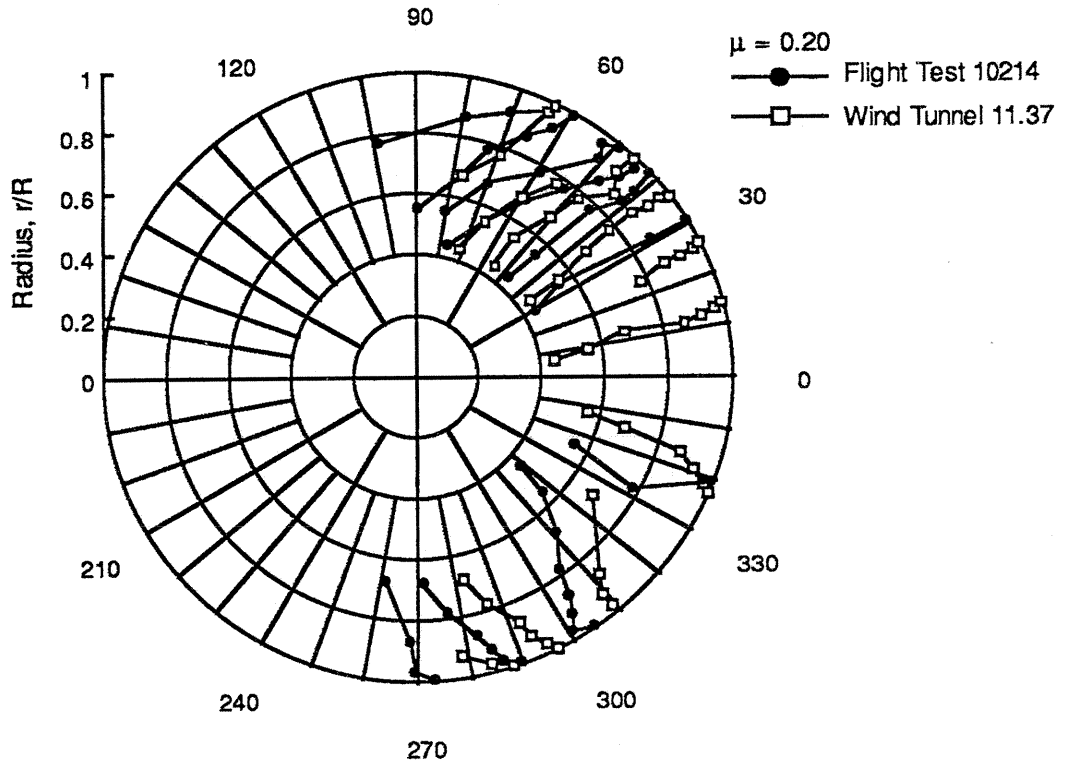

Fig. 10a Comparison of top view BVI locations for $\mu = 0.15$ and 0.20.

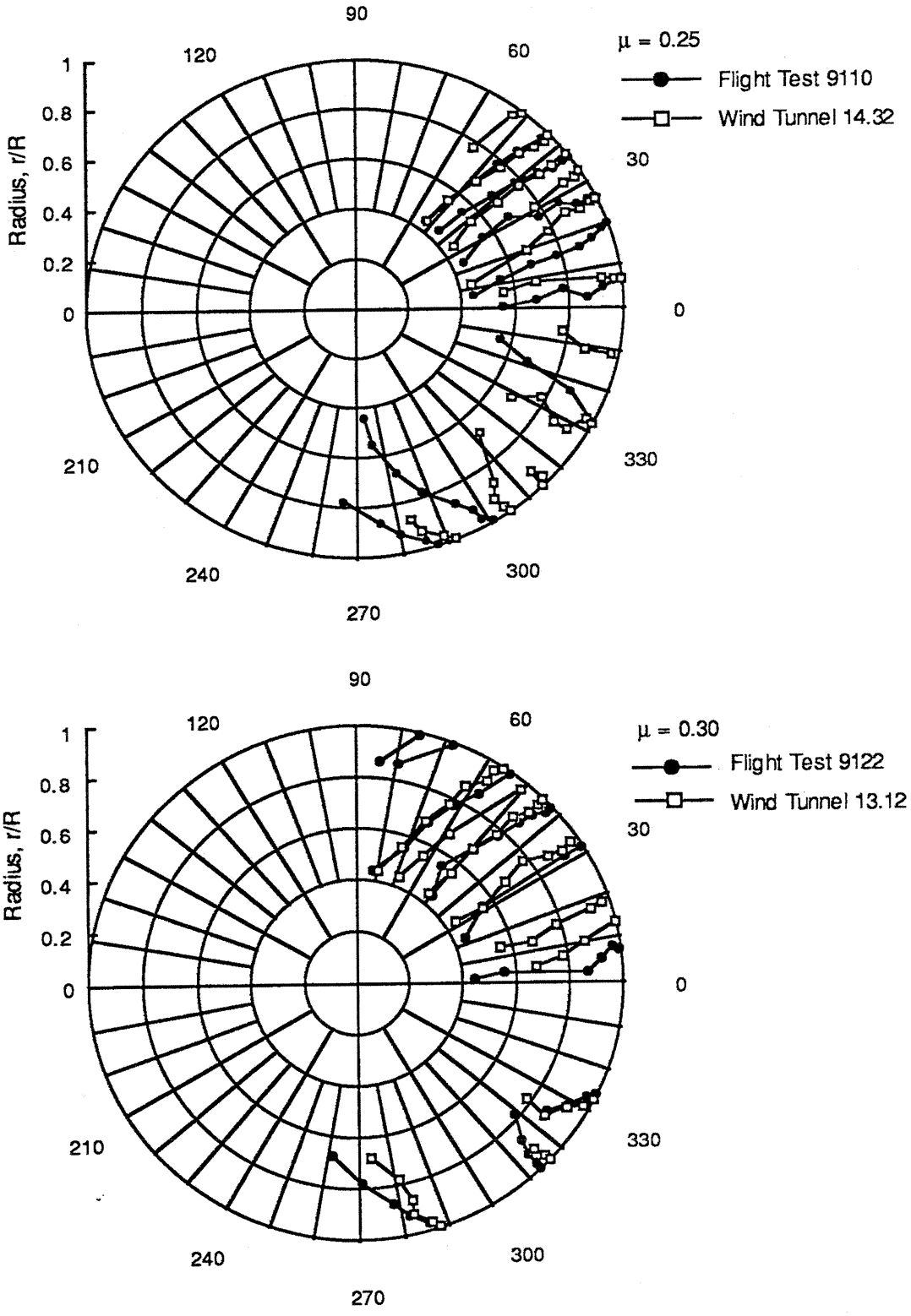

Fig. 10b Comparison of top view BVI locations for $\mu = 0.25$ and 0.30.